Single-particle fusion of influenza viruses reveals complex interactions with target membranes

van der Borg, Guus; Braddock, Scarlett; Blijleven, Jelle; van Oijen, Antoine; Roos, Wouter

Published in:
Journal of Physics-Condensed Matter

DOI:
10.1088/1361-648X/aabc21

Publication date:
2018

Journal of Physics: Condensed Matter

Single-particle fusion of influenza viruses reveals complex interactions with target membranes

To cite this article before publication: Guus van der Borg *et al* 2018 *J. Phys.: Condens. Matter* in press https://doi.org/10.1088/1361-648X/aabc21

Single-Particle Fusion of Influenza Viruses Reveals Complex Interactions with Target Membranes

Guus van der Borg[1], Scarlett Braddock[1], Jelle S. Blijleven[1], Antoine M. van Oijen[2], and Wouter H. Roos[1*]

[1] *Moleculaire Biofysica, Zernike Instituut, Rijksuniversiteit Groningen, The Netherlands*

[2] *School of Chemistry, University of Wollongong, Wollongong, Australia*

** To whom correspondence should be addressed: w.h.roos@rug.nl*

Abstract

The first steps in infection of influenza A virus is contact with the host cell membrane, with which it later fuses. The composition of the target bilayer exerts a complex influence on both fusion efficiency and time. Here, an in vitro, single-particle approach is used to study this effect. Using total internal reflection fluorescence (TIRF) microscopy and a microfluidic flow cell, the hemifusion of single virions is visualized. Hemifusion efficiency and kinetics are studied while altering target bilayer cholesterol content and sialic-acid donor. Cholesterol ratios tested were 0%, 10%, 20%, and 40%. Sialic-acid donors GD1a and GYPA were used. Both cholesterol ratio and sialic-acid donors proved to have a significant effect on hemifusion efficiency. Furthermore, comparison between GD1a and GYPA conditions shows that the cholesterol dependence of the hemifusion time is severely affected by the sialic-acid donor. Only GD1a shows a clear increasing trend in hemifusion efficiency and time with increasing cholesterol concentration of the target bilayer with maximum rates for GD1A and 40% cholesterol. Overall our results show that sialic acid donor and target bilayer composition should be carefully chosen, depending on the desired hemifusion time and efficiency in the experiment.

Introduction

Influenza A is an enveloped, negative-sense single-stranded-RNA virus, member of the Orthomyxoviridae family, and a major cause of epidemics in humans [1, 2]. Enveloped viruses have a lipid bilayer which has to merge with that of the target cell, a step which is crucial to the viral infection pathway [3]. In the influenza infection pathway virions first get internalized by the cell through endocytosis. This internalization is highly cell-type dependent: viruses can enter by clathrin-dependent and clathrin-independent endocytosis, but also by macropinocytosis [4]. After transport of the virus through the endosomal network of the host cell, the low-pH environment in the late endosome triggers the onset of membrane fusion of the viral and endosomal membranes [5]. Following the membrane merging and opening of a pore, the viral genome and its associated proteins are released into the cytosol. Release into the cytosol allows the viral ribonucleoprotein (vRNP) complexes to travel to the nucleus and use the host cell replication mechanisms to produce new viral genome and finally virions [2].

The viral lipid membrane contains the viral membrane proteins hemagglutinin (HA) and neuraminidase (NA). Currently, 16 different subtypes of HA and 9 different subtypes of NA have been classified, of which the strains containing subtypes H1N1, H3N2 and H2N2 have been reported to circulate amongst the human population [2, 6, 7]. NA is important for the budding of new virus particles, whereas the homotrimeric HA protein plays a crucial role in entry into the host cell, being responsible for both attachment and catalysis of membrane fusion, a process that is thermodynamically favorable but has appreciable kinetic barriers [8]. Antigenic shift and antigenic drift are the major causes of yearly influenza epidemics and is therefore studied intensively [9]. HA is proteolytically cleaved from the inactive precursor HA0 into the disulfide-linked subdomains HA1 and HA2 by host cell enzymes [2, 6, 10, 11]. HA1 forms a globular, receptor-binding domain binding to α-sialic-acid linkages present on the host cell membrane [9]. In general, these sialic-acids are a part of a sugar chain on a glycosylated protein or lipid in the host cell membrane. In the prefusion state, HA1 envelopes HA2 and thereby may sterically restrict HA2 rearrangements [9]. The low-pH environment in the late endosome triggers a conformational change in HA. Upon lowering of the pH, HA1 dissociates and HA2 unfolds [12]. Due to the extended intermediate, the fusion peptide can insert into the target membrane. HA then zippers up onto itself which brings the membranes together. The zippering of the HA then forces the membranes to fuse and that leads to the formation of a hemifusion stalk where only the proximal leaflets of both membranes have merged. The stalk can proceed to a fusion pore, or form an elongated hemifusion diaphragm that may then lead to a pore [6, 13].

Fusion kinetics, however, do not depend only on HA. It is also greatly affected by the lipid composition of both the viral particle and the target membrane [14-16]. In this study we investigate the effect of both the sialic-acid donor and the lipid-to-cholesterol ratio of the target membrane on the efficiency and kinetics of influenza fusion using a single-particle *in vitro* assay. The effect of cholesterol on influenza fusion has been studied before using bulk liposomal fusion studies, but the effects at the single-particle level have not yet been elucidated [15, 17]. Furthermore, there have not yet been systematic studies into the effect of the sialic-acid donors. Here we show that both cholesterol percentage and sialic-acid donors have a significant impact on the efficiency as well as the kinetics of influenza hemifusion.

Materials and methods

Viral particle preparation

The PR8 and X-31 strains of Influenza A were purchased from Charles River Labs. Viral particles were diluted in a PBS (pellets, Sigma-Aldrich) + 0.2 mM EDTA (Promega) solution (pH ~7.4) to a concentration of 0.25 mg/ml viral protein. Subsequently the viral particles were labeled using Octadecyl Rhodamine B Chloride (R18; Fisher Scientific) dissolved in DMSO by incubating it with the viral particle suspension at a final concentration of 3 µM. Incubation was performed for 3 hours at room temperature. In order to remove any unincorporated dye a gel filtration column was used (PD-10 desalting column; GE healthcare). The concentration of the fractions was estimated by observing the fractions under the microscope. The fractions with the highest concentrations of viral particles were combined and used for the experiment.

(Proteo-)liposome preparation

Glycophorin A (GYPA) proteoliposomes were prepared using a mixture of 1,2-dioleoyl-sn-glycero-3-phosphocholine (DOPC), Cholesterol, and 1,2-dioleoyl-sn-glycero-3-phosphoethanolamine-N-(biotinyl) (biotin-PE). The used molar ratio was 60/80/90/100 : 40/20/10/0 : $2.5 \cdot 10^{-3}$ of DOPC : Cholesterol : Biotin-PE with the DOPC : Cholesterol ratios depending on the desired cholesterol content of the target membrane. All lipids were dissolved in chloroform and purchased from Avanti Polar Lipids. Liposomes were made in a solution of PBS+0.2 mM EDTA to a final concentration of 7 mM. Liposome formation was done through a freeze-thaw extrusion procedure using a 200 nm diameter pore filter (Avanti). Extrusion was performed at 40°C. GYPA insertion was performed using detergent. Detergent was added to the liposome suspension followed by GYPA (Sigma-Aldrich) in a molar ratio of $2.5 \cdot 10^{-3}$ after which the detergent was removed using Biobeads (Bio-rad).

Ganglioside G_{D1a} (GD1a) liposomes were prepared using the same protocol with a few exceptions. No insertion was necessary as GD1a could be added together with the other lipids. The used molar ratio was 60/80/90/100 : 40/20/10/0 : $2.5 \cdot 10^{-3}$: 1 of DOPC : Cholesterol : Biotin-PE : GD1a (Sigma-Aldrich). The extrusion filter used had a pore diameter of 100 nm.

Fusion assay

Glass coverslips were cleaned using 30 min of sonication in acetone and ethanol followed by 10 min sonication in 1M KOH. In between sonication the coverslips were rinsed with deionized water. Coverslips were dried overnight at 110°C. Before use, coverslips were cleaned in an oxygen plasma cleaner for 30 min and attached to the flow cells.

Polydimethylsiloxane (PDMS) flow cells were made by pouring PDMS over a mold and curing it to harden it. The flow cell consists of 5 separate channels with a width and height of 0.5 x 0.2 mm. The setup was placed on a home-built total internal reflection fluorescence (TIRF) microscope, using an inverted microscope (IX-71; Olympus) and a high numerical aperture, oil-immersion objective (NA 1.45, ×60; Olympus). Lipid bilayers were formed by filling the microfluidic channels with the (proteo-) liposome suspension and incubating for 45 min. After rinsing with PBS+0.2 mM EDTA labeled viral particles were docked to the bilayer. Fluorescein- labelled streptavidin (Life Technologies) was bound to the biotin-PE as a pH sensor. The system was acidified to a pH of 5.0 by using citric acid buffer. The fluorophores were excited using 488 and 561 nm lasers (Coherent). Viral membrane fluorescence (red) and fluorescein pH drop fluorescence (green) were projected on different halves of an EM-CCD camera (Hamamatsu). Videos of 1200 frames of 200 ms each were taken for a total movie length of 4 min.

FRAP

In order to confirm the fluidity off the lipid bilayers Fluorescence Recovery After Photobleaching (FRAP) experiments were performed. In order to do this liposomes were made which included 1 µM R18 in ethanol during lipid mixing. These were used to form a lipid bilayer in the same way as during a fusion assay. An aperture and high laser power was used to bleach an area of the lipid bilayer after which recovery was assessed.

Analysis

Home-written Matlab scripts were used to analyze the fusion process. The fluorescein fluorescence emission was fitted with the following function:

$$f(t) = y_{offset} + \frac{h}{2} erfc\left(\frac{t - t_c}{\frac{w}{2}}\right)$$

In which h is the height of the intensity drop, w is the width of the transition, t_c is the time at which the transition is half complete, and y_{offset} is the residual intensity after dissipation. The time of pH drop (t_0) was defined as ($t_c + w/2$), when fluorescein fluorescence is at ~8%.

$t_{hemifusion}$ was determined by using matlab to generate fluorescence over time graphs for every individual particle and then manually designating the onset of the peak in each graph.

The statistical significance of the hemifusion efficiency was tested by comparing the mean using a Tukey test (SI table 1). The statistical significance of the hemifusion time was tested by comparing the medians using a Wilcoxon rank sum test (SI table 2).

Results

Hemifusion was studied using two commonly used influenza A virus strains: PR8 (H1N1) and X-31 (H3N2). Single influenza virus particles were immobilized on a supported planar lipid bilayer using either GYPA or GD1a as sialic-acid receptor and were fluorescently labeled in the membrane with a lipophilic dye, R18 (fig. 1A). The target bilayers contained 0, 10, 20, or 40 percent mol/mol cholesterol and imaging was performed using TIRF microscopy (fig. 1B). The fluidity of the bilayer was confirmed using FRAP in a separate experiment (SI fig. 1). The experiment starts with flowing in the virus particles which dock onto the sialic-acid donors. As the pH is still too high (pH ~7.4), no fusion can occur. Only after flowing in citric acid buffer (pH 5.0), the pH is lowered and hemifusion can start to occur. The pH drop, after flowing in the citric acid buffer, is monitored by labeling the target membrane with fluorescein. When the pH is lowered, the pH-sensitive fluorescence of fluorescein drops, indicating the time of the hemifusion trigger (t_0). Hemifusion itself is visualized by the diffusion of the R18 membrane label from the virus into the target membrane. R18 can start to diffuse after the fusion of the proximal leaflets. As R18 is a self-quenching dye this diffusion is characterized by an initial spike in fluorescence followed by a gradual decrease in the region of interest. The onset of this 'spike' is defined as the hemifusion time ($t_{hemifusion}$) (fig. 1C).

Hemifusion efficiency is defined as the fraction of particles that undergo hemifusion within the field of view and during the time of the experiment (5 minutes). In all conditions hemifusion efficiency was affected by the cholesterol percentage of the target bilayers. All conditions show an upward trend in hemifusion efficiency as the percentage of cholesterol in the target bilayer increased (fig. 2A). This upward trend is best illustrated by the results of the X-31 GD1a condition where all of the

tested cholesterol conditions showed a significant change in efficiency (SI table 1). This change in efficiency, however, seems to be less pronounced in the conditions which use GYPA as a sialic-acid donor. For both X-31 and PR8 the 0% and 10% cholesterol conditions do not show a significant difference. Also of note, the hemifusion efficiency of the GD1a condition is significantly higher overall than in the GYPA conditions. The higher efficiency of GD1a suggests that the sialic-acid donor also has an impact on the hemifusion efficiency. It also shows that the sialic-acid donor has an effect on the cholesterol dependency of hemifusion efficiency. As a control, experiments were performed with Influenza X-31 and lowered concentrations of GD1a. Trials were performed with 50x less and 400x less GD1a in target bilayers with a 40% cholesterol content. 40% was chosen as this was the condition closest to natural endosomes [18, 19]. The rationale behind using conditions with 50x less and 400x less GD1a is that these concentrations result in the target bilayer having the same concentration of sialic-acid or sialic-acid donors respectively as the GYPA condition. As GD1a is used in a 400x times higher concentration and GYPA has 8x as many sialic-acids as GD1a (GYPA has 16, GD1a has 2) [20, 21]. Both 50x less and 400x less showed hemifusion efficiency comparable to the GYPA condition (SI fig. 2).

While there was an observable trend in all conditions when looking at hemifusion efficiency, this does not seem to be the case for hemifusion time, the time between t_0 and $t_{hemifusion}$. Both of the GYPA conditions do not show a trend when comparing the mean hemifusion times to the percentage of cholesterol in the target bilayer (fig. 2B). The condition with GD1a however shows a very clear trend. The cumulative fusion efficiency plots of the data shows that the time of hemifusion becomes higher as cholesterol content of the lipid bilayer increases (fig. 3, SI fig. 3&4). This difference between GD1a and GYPA conditions, again, implies that the sialic-acid donor has an effect on the cholesterol dependence of hemifusion. The control with lowered GD1a did not show a conclusive effect of sialic-acid concentration on the hemifusion time (SI fig. 5).

Discussion

The increase in hemifusion efficiency at higher cholesterol levels has already been documented in the bulk studies by Domanska et al. [17] As they postulate, it is very likely that the effect of cholesterol on the intrinsic curvature of the membrane plays a role, as fusion proceeds via strongly curved intermediate states [22]. Cholesterol would aid the fusion process as its negative curvature would lower the energy necessary to form the intermediate state [23, 24]. While it is very likely that the negative curvature of cholesterol plays a large role in the increase of hemifusion efficiency it is also likely it is not the only effect of cholesterol. In this study we could see that the cholesterol dependency of hemifusion efficiency was modulated by the sialic-acid donors, with the GYPA conditions showing a significantly lower response to changes in the composition of the target membrane compared to the GD1a condition especially at low cholesterol contents. One explanation for this sialic-acid dependency is that cholesterol may interact with the sialic-acid donors, possibly forming lipid rafts in one or both of the conditions [25-27]. This recruitment may form a high cholesterol area which is either enriched or depleted of sialic-acids which, in turn, could increase or decrease the probability of the influenza viral particle docking on to the membrane. For instance, the lower cholesterol dependency on hemifusion efficiency of the GYPA condition could mean that GYPA recruits cholesterol in lipid rafts and thus reduces the relative difference of cholesterol content in specific sialic-acid rich areas between the trials with differing overall cholesterol contents.

The effect of the sialic-acid donor on the hemifusion efficiency is not well documented nor well standardized for experiments. Studies into the fusion of influenza vary in the use of sialic-acid donors

[6, 14, 17, 28]. Yet we find a remarkable effect on both hemifusion efficiency and time when comparing the GYPA and GD1a conditions. Possibly the increased efficiency in hemifusion in the GD1a condition was based on the difference in sialic-acid concentration. When forming our bilayers GYPA and GD1a were added in concentrations following the protocols of Otterstrom et al. and Floyd et al., respectively [6, 28]. However, these studies do not use equivalent concentrations of sialic-acid with Floyd using 50× more sialic-acid in the bilayer. We tested the different sialic-acid concentrations in the 40% cholesterol condition. The low GD1a conditions showed hemifusion efficiency that reached similar levels as in the GYPA condition (SI fig. 2). This effect of low GD1a concentration would mean that sialic-acid concentration is an important parameter in hemifusion efficiency. However, it is also likely that the type of donor plays a role as well. For example, one GYPA glycoprotein has on average 16 sialic-acids while one GD1a molecule merely contains two [20, 21]. This difference in sialic-acids per molecule could mean that effectively the sialic-acid concentration of GYPA could be higher due to a higher local concentration which could have an impact on HA binding.

The effect of the sialic-acid donor is further seen when studying its effect on hemifusion time. As neither the X-31 GYPA nor the PR8 GYPA conditions show any sort of cholesterol dependent trend in their hemifusion times while the GD1a condition does. Yet, in the model proposed by Ivanovic et al. the hemifusion efficiency and time are correlated to one another [1, 8]. It is possible that the increased cholesterol content stabilizes the hemifusion intermediate or that it increases HA insertion probability. Both of which could result in the process going much faster [23, 24].

The fact that in the GYPA conditions the hemifusion time does not show a cholesterol dependent trend is therefore very much of interest. Our GYPA data does not show any correlation between hemifusion efficiency and hemifusion time. Therefore, it is likely that there is a factor which does affect hemifusion efficiency but not the hemifusion time and that this factor is a property of the target bilayer, a factor which still seems to be missing from the current models. A proposition made more likely when looking at the low GD1a results as once again the hemifusion efficiency and the time do not seem to be correlated. In the case of the comparable concentrations of sialic-acid (50x less) we notice a marked drop in hemifusion efficiency, yet the hemifusion time is actually higher than in the regular concentration (SI fig. 5). The hemifusion time with the 400x less GD1a condition is increased yet in this condition particle docking within field of view was an order of magnitude lower than other conditions. As such, the significance of this result is debatable.

It is possible that an all-or-nothing effect may be at play here. The observed results could be explained by GYPA recruiting cholesterol into cholesterol and sialic-acid enriched areas which greatly increase the probability of HA2 insertion into the target membrane. These enriched areas would make for very hemifusion efficient ‘hotspots’. These hotspots would explain the lack of cholesterol dependence in GYPA hemifusion rates. If hotspots have similar local concentrations of cholesterol across the conditions it would remove cholesterol as a factor when studying hemifusion time. It would also explain why hemifusion efficiency would still be cholesterol dependent as opposed to the time. As the overall cholesterol content of the bilayer increased the surface area covered by these hotspots would as well. The increased hotspot surface area, in turn, would increase the probability of virions docking on or near these hotspots. As the vast majority of hemifusion events would be on or near these hotspots this would increase hemifusion efficiency overall.

Conclusion

This study shows that both the sialic-acid donor and the cholesterol ratio of the target bilayer has a significant effect on the hemifusion efficiency of Influenza viral particles. However, unlike current models this effect on hemifusion efficiency does not necessarily correlate to hemifusion time. This

lack of correlation shows that there still is a parameter that the current models do not account for, a parameter involving the composition of the target membrane. Our study also reveals that for a profound description of fusion dynamics, the role of the used receptor molecule has to be taken into account.

Acknowledgements

WHR acknowledges funding via a Nederlandse organisatie voor Wetenschappelijk Onderzoek VIDI grant and a FOM-Projectruimte grant.

References

1. Ivanovic T, Harrison SC. Distinct functional determinants of influenza hemagglutinin-mediated membrane fusion. Elife. 2015 Nov 27;4:e11009.

2. Hamilton BS, Whittaker GR, Daniel S. Influenza virus-mediated membrane fusion: determinants of hemagglutinin fusogenic activity and experimental approaches for assessing virus fusion. Viruses. 2012 Jul;4(7):1144-68.

3. Banerjee I, Miyake Y, Nobs SP, Schneider C, Horvath P, Kopf M, et al. Influenza A virus uses the aggresome processing machinery for host cell entry. Science. 2014 Oct 24;346(6208):473-7.

4. de Vries E, Tscherne DM, Wienholts MJ, Cobos-Jimenez V, Scholte F, Garcia-Sastre A, et al. Dissection of the influenza A virus endocytic routes reveals macropinocytosis as an alternative entry pathway. PLoS Pathog. 2011 Mar;7(3):e1001329.

5. Boonstra S, Blijleven JS, Roos WH, Onck PR, van der Giessen E, van Oijen AM. Hemagglutinin-mediated Membrane Fusion: a Biophysical Perspective. Annual Reviews of Biophysics submitted.

6. Floyd DL, Ragains JR, Skehel JJ, Harrison SC, van Oijen AM. Single-particle kinetics of influenza virus membrane fusion. Proc Natl Acad Sci U S A. 2008 Oct 7;105(40):15382-7.

7. Gaur P, Munjhal A, Lal SK. Influenza virus and cell signaling pathways. Med Sci Monit. 2011 Jun;17(6):54.

8. Ivanovic T, Choi JL, Whelan SP, van Oijen AM, Harrison SC. Influenza-virus membrane fusion by cooperative fold-back of stochastically induced hemagglutinin intermediates. Elife. 2013 Feb 19;2:e00333.

9. Lin X, Noel JK, Wang Q, Ma J, Onuchic JN. Lowered pH Leads to Fusion Peptide Release and a Highly Dynamic Intermediate of Influenza Hemagglutinin. J Phys Chem B. 2016 Sep 15;120(36):9654-60.

10. Skehel JJ, Wiley DC. Receptor binding and membrane fusion in virus entry: the influenza hemagglutinin. Annu Rev Biochem. 2000;69:531-69.

11. Russell CJ. Acid-induced membrane fusion by the hemagglutinin protein and its role in influenza virus biology. Curr Top Microbiol Immunol. 2014;385:93-116.

12. Lin X, Eddy NR, Noel JK, Whitford PC, Wang Q, Ma J, et al. Order and disorder control the functional rearrangement of influenza hemagglutinin. Proc Natl Acad Sci U S A. 2014 Aug 19;111(33):12049-54.

13. Harrison SC. Viral membrane fusion. Virology. 2015 May;479-480:498-507.

14. Domanska MK, Dunning RA, Dryden KA, Zawada KE, Yeager M, Kasson PM. Hemagglutinin Spatial Distribution Shifts in Response to Cholesterol in the Influenza Viral Envelope. Biophys J. 2015 Nov 3;109(9):1917-24.

15. Biswas S, Yin SR, Blank PS, Zimmerberg J. Cholesterol promotes hemifusion and pore widening in membrane fusion induced by influenza hemagglutinin. J Gen Physiol. 2008 May;131(5):503-13.

16. Zawada KE, Wrona D, Rawle RJ, Kasson PM. Influenza viral membrane fusion is sensitive to sterol concentration but surprisingly robust to sterol chemical identity. Sci Rep. 2016 Jul 19;6:29842.

17. Domanska MK, Wrona D, Kasson PM. Multiphasic effects of cholesterol on influenza fusion kinetics reflect multiple mechanistic roles. Biophys J. 2013 Sep 17;105(6):1383-7.

18. Crane JM, Tamm LK. Role of cholesterol in the formation and nature of lipid rafts in planar and spherical model membranes. Biophys J. 2004 May 01;86(5):2965-79.

19. Guha S, Rajani M, Padh H. Identification and characterization of lipids from endosomes purified by electromagnetic chromatography. Indian J Biochem Biophys. 2007 December 01;44(6):443-9.

20. Tomita M, Marchesi VT. Amino-acid sequence and oligosaccharide attachment sites of human erythrocyte glycophorin. Proc Natl Acad Sci U S A. 1975 Aug;72(8):2964-8.

21. Liang S, Wang M, Tapping RI, Stepensky V, Nawar HF, Triantafilou M, et al. Ganglioside GD1a is an essential coreceptor for Toll-like receptor 2 signaling in response to the B subunit of type IIb enterotoxin. J Biol Chem. 2007 March 09;282(10):7532-42.

22. Chernomordik LV, Kozlov MM. Mechanics of membrane fusion. Nat Struct Mol Biol. 2008 Jul;15(7):675-83.

23. Kozlovsky Y, Kozlov MM. Stalk model of membrane fusion: solution of energy crisis. Biophys J. 2002 Feb;82(2):882-95.

24. Chen Z, Rand RP. The influence of cholesterol on phospholipid membrane curvature and bending elasticity. Biophys J. 1997 Jul;73(1):267-76.

25. Baier CJ, Fantini J, Barrantes FJ. Disclosure of cholesterol recognition motifs in transmembrane domains of the human nicotinic acetylcholine receptor. Sci Rep. 2011;1:69.

26. Fantini J, Barrantes FJ. How cholesterol interacts with membrane proteins: an exploration of cholesterol-binding sites including CRAC, CARC, and tilted domains. Front Physiol. 2013 Feb 28;4:31.

27. Kiessling V, Crane JM, Tamm LK. Transbilayer effects of raft-like lipid domains in asymmetric planar bilayers measured by single molecule tracking. Biophys J. 2006 Nov 1;91(9):3313-26.

28. Otterstrom JJ, Brandenburg B, Koldijk MH, Juraszek J, Tang C, Mashaghi S, et al. Relating influenza virus membrane fusion kinetics to stoichiometry of neutralizing antibodies at the single-particle level. Proc Natl Acad Sci U S A. 2014 Dec 2;111(48):5143.

Figure legends

Figure 1: Experimental setup. A) Schematic representation of viral particle and lipid bilayer. A planar lipid bilayer is formed over a glass surface as a target bilayer. Labeled viral particles are docked and the target bilayer is labeled with a pH sensor. The membrane dye (R18) is indicated as red, the pH sensor (fluorescein) is indicated as green. As pH drops Fluorescein quenches and upon hemifusion the membrane dye diffuses across the planar bilayer. B) A schematic representation of the microscope setup. Experiments were performed in separate channels of the microfluidic flow cell. Emitted fluorescence is split using a dichroic mirror and imaged on different halves of an EM-CCD camera. C) Field of view and resulting graphs. (Top left). Microscope image 5 s before pH trigger. Green channel shows fluorescein, red channel shows the viral particles. (Top right). Microscope image 240 s after pH drop. Fluorescein signal has lowered and particles have undergone hemifusion. (Bottom). The resulting graph after analysis. The drop in fluorescence in the green channel is designated t_0. A spike in fluorescence in the red channel indicates the $t_{hemifusion}$ of the particle.

Figure 2: Hemifusion efficiency and hemifusion time. A) The hemifusion efficiency of the different conditions. Dots are individual experiments and represent the fraction of particles that underwent hemifusion. Weighted median (line) and weighted mean (circle) are shown. Median and mean weighted to the number of particles in a trial. B) The hemifusion times of the different conditions. Dots are the median hemifusion time of the individual experiments. The median (line) and mean (circle) hemifusion times of the pooled experiments are shown. (Numerical values of mean and median hemifusion time in SI table 3)

Figure 3: The cumulative distribution of hemifused particles over time in the X-31 GD1a condition. Data points represent individual viral particles. Hemifusion times of viral particles were pooled and normalized. The data was fitted with the commonly used gamma distribution fit in order to illustrate the changes in hemifusion time [6]. Fit parameters in SI table 4.

Figures

Figure 1:

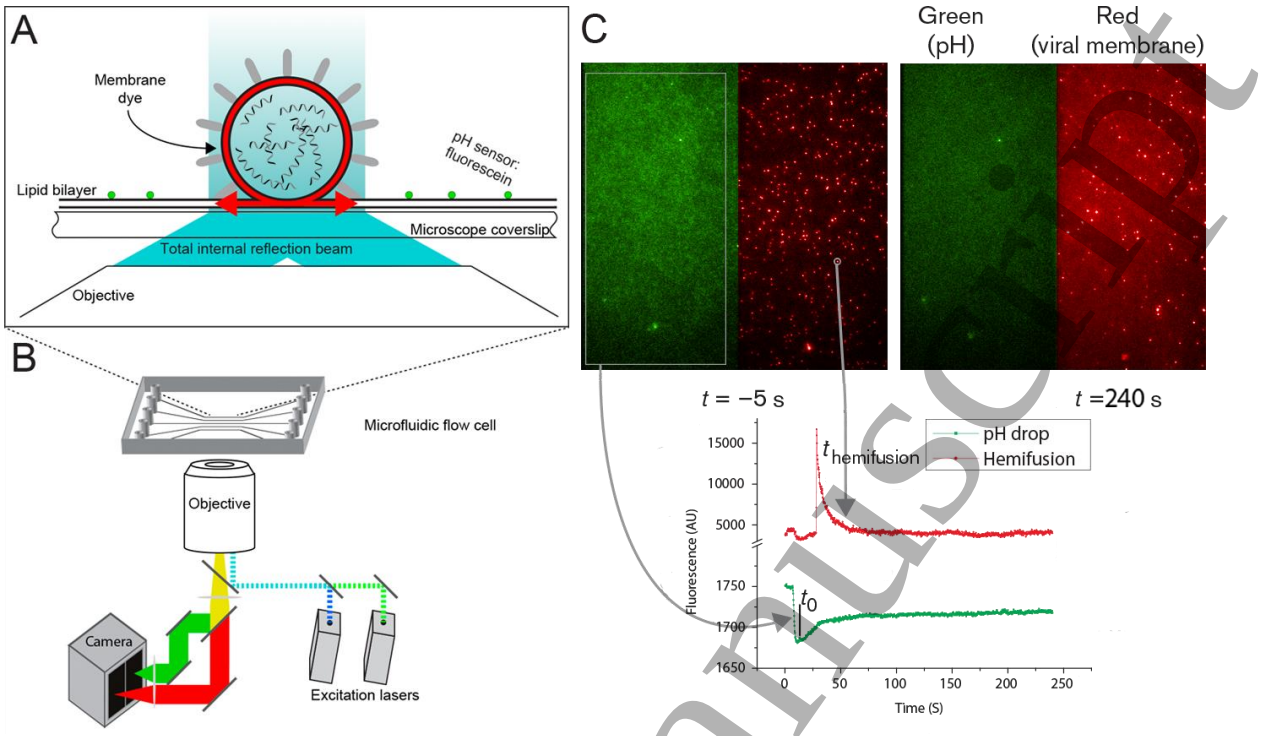

Figure 2:

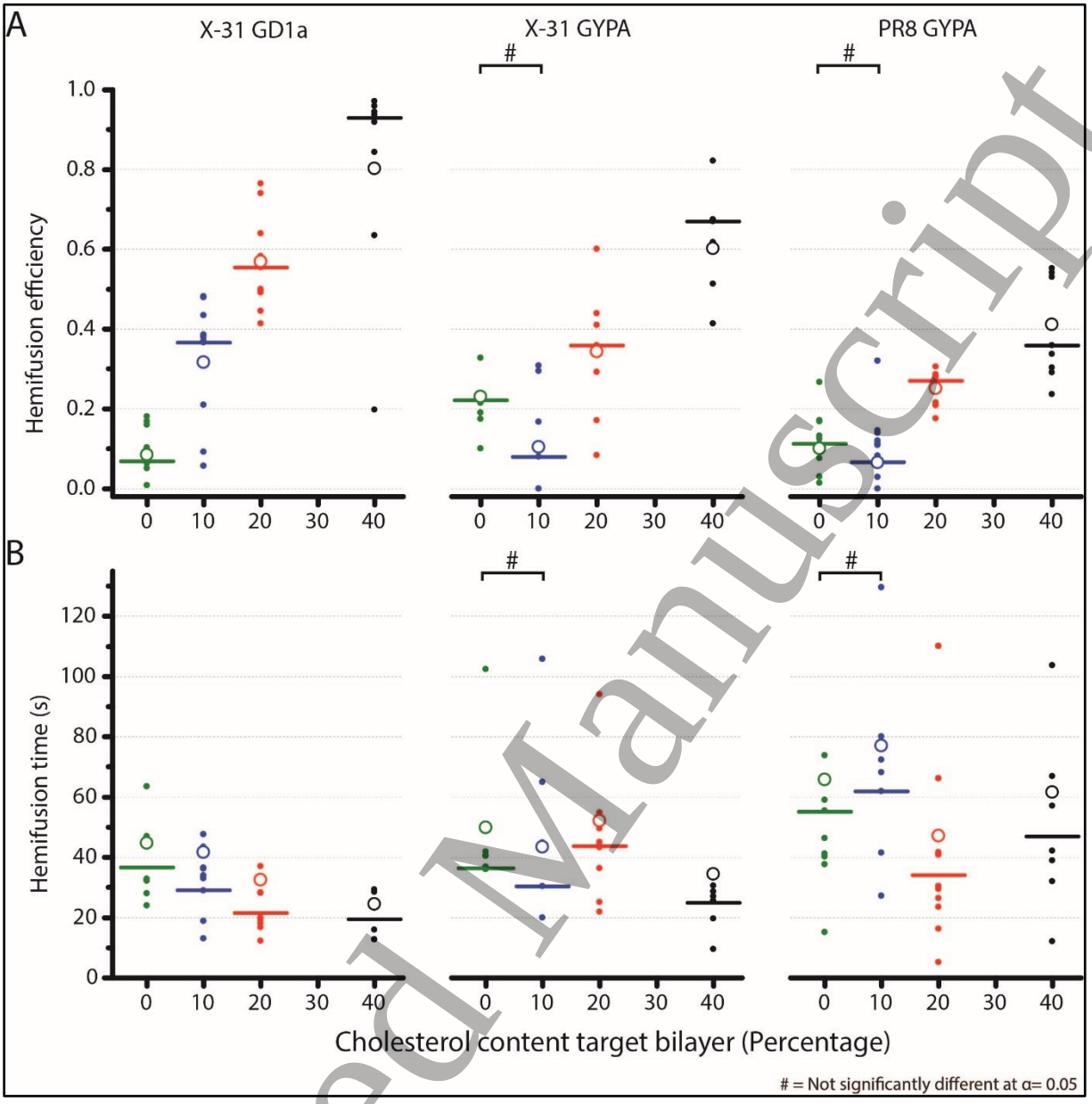

Figure 3: